Int. J. Electrochem. Sci., 14 **(2019)** 5472 – 5482, doi: 10.20964/2019.06.44

International Journal of
ELECTROCHEMICAL
SCIENCE
www.electrochemsci.org

Electrochemical Oxidation Products of Piperazine as Corrosion Inhibitor for HP13Cr Steel in 20% HCl Solution

Jun Zhao[1], *Juantao Zhang*[2,*], *Junfeng Xie*[3], *Hualong Yang*[3], *Wenwen Song*[3] *Youwei Li*[3], *Mifeng Zhao*[3], *Xiaoping Yang*[4]

[1] China United Northwest Institute for Engineering Design and Research Co., Ltd. Xi'an, Shaanxi, P.R. China 710077.
[2] State Key Laboratory for Performance and Structure Safety of Petroleum Tubular Goods and Equipment Materials, Xi'an, Shaanxi, P.R. China 710077.
[3] Petrochina Tarim Oilfield Complany, Korla,Xinjiang, P.R. China 841000.
[4] PetroChina Coalbed Methane Co., Ltd. Beijing, P.R. China 100028.
[*]E-mail: 464932044@qq.com.

Received: 21 January 2019 / *Accepted:* 13 March 2019 / *Published:* 10 May 2019

Three products are synthesized by adjusting current density and quantity of ionic liquid [Bmim][PF_6] in electrochemical oxidation of piperazine. The molecular structures of *N*-methoxyl piperazine, *N*-carbonyl piperazine and *N*, *N'*-dicarbonyl piperazine are determined by infrared spectroscopy and gas chromatography (GC)/mass spectrometry (MS). For application, the inhibition effect of the three products on the corrosion of HP13Cr steel in 20% (weight %) HCl solution was studied by means of weight loss and polarization measurements. The experiments revealed that *N*-carbonyl piperazine and *N*, *N'*-dicarbonyl piperazine show 91.0% and 95.2% inhibition efficiencies respectively at the concentration of 3% (weight %). However, the product of *N*-methoxyl piperazine has no inhibition behavior.

Keywords: Electrochemical synthesis; ionic liquid; acid inhibition.

1. INTRODUCTION

Ionic liquids are increasingly recognized and accepted as novel, green solvents and catalysts with great application potential in electrochemistry, catalysis, synthesis and separation based on their special physical and chemistry properties. The use of ionic liquid as an addition has been researched by many authors. A.F. Zanette, [1] Z. Yang [2] and I. Kaleem [3] used ionic liquids as a biotransformation medium due to their excellent enzyme activity, stability, and selectivity. Y.B. Wei, [4] D. Zhao, [5] X.D. Lang [6] and B. Dong [7] accomplished organic synthesis research in ionic liquid solvents. Ionic liquids are also used as electrolytes in electrosynthesis.[8-10] Compared to volatile organic solvents,

ionic liquids are currently more widely used as solvents due to their wider liquid range, neglectable vapor pressure, and good reusability, which is very important as environmental problems become increasingly concerning.[11-15]

A completely ionic composition is a significant feature of ionic liquids that enables them to have excellent conductivity,[16-17] thus making ionic liquids potentially "green" electrochemical materials. In this study, the objective products are obtained by adjusting the quantity of ionic liquid [Bmim][PF_6], and the current density in electrochemical oxidation of piperazine. The electrochemical oxidation process is synchronously monitored by a react-infrared (ReactIR) reaction analysis system, and the molecular structures of the three products are characterized by GC/MS. For application, the inhibition effect of the three products on the corrosion of HP13Cr stainless steel in 20% (weight %) HCl aqueous solution is studied by weight loss and potentiodynamic polarization measurements.

2. EXPERIMENTAL

2.1. Materials and apparatus

The testing materials are HP13Cr (manufactured by JFE Steel Co., Japan) oil tube steel discs with the chemical composition of (wt %): C 0.011, Mn 0.49, Si 0.30, S 0.0035, P 0.023, Cr 13.46, Mo 1.93, Ni 6.19, V 0.051, Ti 0.096, Cu 0.36 and balanced Fe.

The reaction products are determined by ReactIR Reaction Analysis System made by Mettler-Toledo Co., Switzerland, gas chromatography (Agilent 6890) /mass spectrometry (Hewlett–Packard 5973), and H-nuclear magnetic resonance spectrometer (HNMR, INOVA-400MHz, Varian, USA). The potentiodynamic polarization measurement is performed on a M273A potentiostat (Princeton instrument Co., USA) attached with a M5210 lock-in amplifier (Princeton instrument Co., USA).

2.2. Synthesis of ionic liquid

First, 41.0 g (0.5 mol) *N*-methylimidazole and 68.5 g (0.5 mol) butyl bromide are blended in a 1000 mL flask and stirred at 70 °C for 2.5 h. Then, 92 g (0.5 mol)/500 mL potassium hexafluorophosphate water solution is added in and allowed to continue to react at 50 °C for 5 h. At the end of the reaction, the solution obviously delaminates. Then, the oil phase is separated, washed using ether and distilled water and vacuum dried at 30 °C for 24 h. Eventually, 245 g buff ionic liquid of [Bmim][PF_6] is obtained. The react equation is shown as follows.

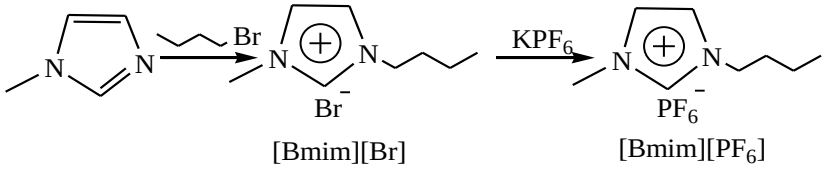

Scheme 1. The reaction approach for the synthesis of [Bmim][PF_6].

2.3. Electrochemical oxidation of piperazine

In the electrochemical oxidation experiment, the 1 L cell is used as reactor. The anode and cathode are graphite plates and are parallel to each other with an inner gap of 1.0 cm. The regulated DC power supply is used to provide a 25 V fixed voltage. None of the experimental process is heated. Then, 50 g piperazine (hexahydrate), 100 mL methanol and 100 mL distilled water are added to the vessel, using a magnetic stirrer (200 rpm) to stir the solution and further homogenize the electrolyte solution. Different quantities of ionic liquid [Bmim][PF_6] are added to the vessel for the purpose of serving as the catalyst and adjusting the current. The electrochemical oxidation reaction process is simultaneously monitored by a ReactIR reaction analysis system every 10 min. After electrolyzing for 2 h, the power supply is switched off and the stirring ceases. When the electrolyte solution is layered in two layers, the ionic liquid is separated, and the product is characterized using GC/ MS. In GC/MS, a low polarity column and high purity helium gas were used; the split ratio was set as 50:1; the sample was diluted ten times with n-hexane; and the testing temperature was first maintained at 45 °C for 3 min, then increased to 280°C in 10 °C increments each minute and was kept at temperature for 5 min.

3. RESULTS AND DISCUSSION

3.1 Infrared spectroscopy monitoring

The electrochemical oxidation reaction process is monitored in real-time by an IR reaction analysis system, and the three-dimensional stack plot is collected every 10 min. The mixed solution of methanol and water is used as the background. Fig. 1, Fig. 2, and Fig. 3 are the three-dimensional stack plots of the IR spectra for *N*-methoxyl piperazine, *N*-carbonyl piperazine, and *N*, *N'*-dicarbonyl piperazine, respectively.

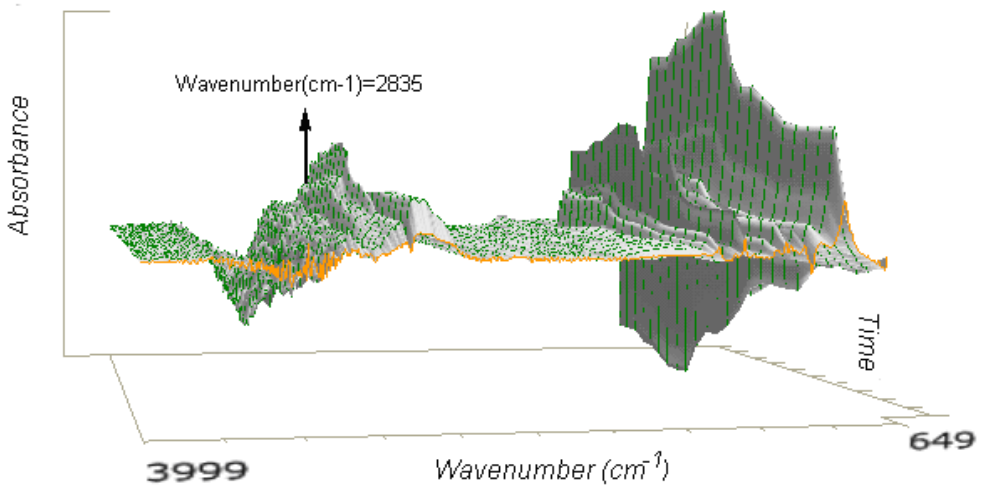

Figure 1. Three-dimensional stack plot of the IR spectra for *N*-methoxyl piperazine.

From Fig. 1, the methoxyl stretching vibration can be seen at the wavenumber of 2835 cm^{-1},

which indicates that the electrolytic product molecule contains methoxyl group. It can be seen form Fig. 2 that the absorbance in the 2700-2800 cm^{-1} region (shown in Fig. 2(a)), which may be the N–H bond stretching vibration, decreased with the reaction time elapsing. The absorbance in 1630-1690 cm^{-1} region (shown in Fig. 2(b)), which may be the C=O stretching vibration, increased from nonexistence at the electrochemical oxidation reaction beginning to 0.38 at the electrochemical oxidation reaction ending.[18-19] In Fig. 3, the absorbance in 1630-1690 cm^{-1} region, which may be the C=O stretching vibration, is stronger than that of Fig. 2. These indicate that the electrolytic products molecule contains C=O group and it has been confirmed by the GC/MS results.

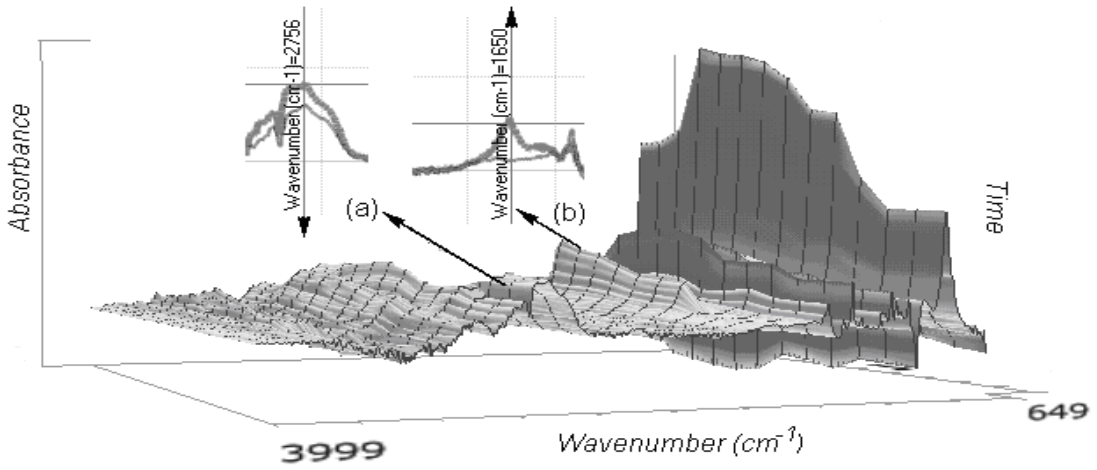

Figure 2. Three-dimensional stack plot of the IR spectra for *N*-carbonyl piperazine.

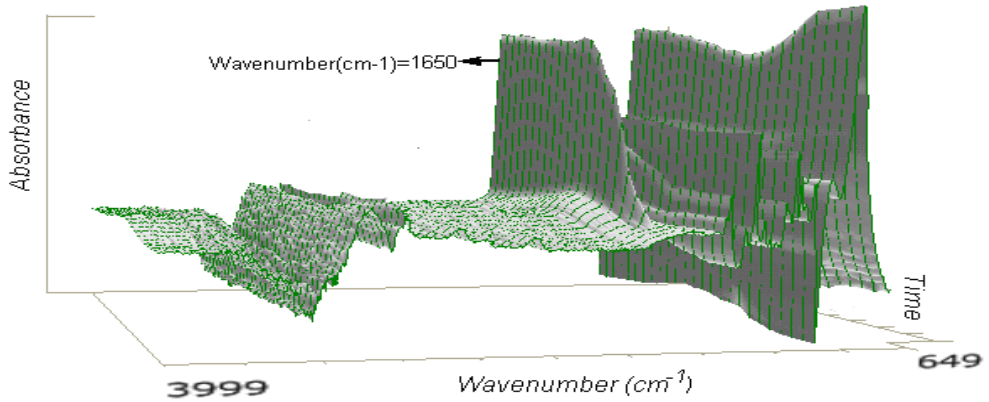

Figure 3. Three-dimensional stack plot of the IR spectra for *N, N'*-dicarbonyl piperazine.

3.2 GC/MS AND HNMR

Table 1 shows the GC/MS and HNMR results of the electrochemical oxidation of piperazine with different quantities of ionic liquid. Fig. 4 is a representative graph of the GC results (the peak of the solvent has been omitted). Fig. 5 presents the possible reaction processes for the three products. From Table 1, the HNMR data indicate that the three products are detected and possess four kinds of H

with different δ, and a corresponding number of peaks are interpreted as *N*-methoxyl piperazine. According to the same argument, the other two products are *N*-carbonyl piperazine and *N, N'*-dicarbonyl piperazine, which is consistent with GC/MS results. Compared with the traditional organic synthesis, the method of this study has the advantages of few steps, short route and mild condition.[20,21] In Fig. 4 and Fig. 5, the product is changed by increasing the quantity of ionic liquid, and three products can be obtained by adjusting the quantity of ionic liquid. The critical quantities of ionic liquid for producing *N*-carbonyl piperazine and *N, N'*-dicarbonyl piperazine are 30 g and 40 g, respectively. The results indicate that the ionic liquid [Bmim][PF_6] may serve as an electrolyte and as a catalyst. Because the current increases as the quantity of ionic liquid increases, the degree of oxidation also increases as the current increases.

Table 1. The GC/MS and HNMR results of the electrochemical oxidation of piperazine for 2 h at 25 V with different quantities of ionic liquid[a]

Electrolytic solution component	Quantity of Ionic liquid (g)	Current (A)	Main products and yield[b]	Current efficiency[c]
50 g piperazine + 100 mL methanol + 100 mL distilled water	0	0.02	piperazine	\
	20	1.00	*N*-methoxyl piperazine (20.3%)	70.1%
	25	1.26	*N*-methoxyl piperazine (32.6%)	89.6%
	30	1.54	*N*-carbonyl piperazine (17.1%)	76.3%
	35	1.78	*N*-carbonyl piperazine (24.4%)	94.7%
	40	2.02	*N,N'*-dicarbonyl piperazine (12.1%)	82.9%
	45	2.23	*N,N'*-dicarbonyl piperazine (15.7%)	93.8%

[a] GC/MS spectrum, 70 eV, M/e (relative intensity): piperazine: 86 M^+(63), 71(29), 57(69), 44(100), 29(75), 18(14); *N*-methoxyl piperazine: 116 M^+(45), 101(13), 85(63), 69(71), 56(100), 44(74), 29(44), 15(7); *N*-carbonyl piperazine: 114 M^+(43), 97(18), 85(46), 69(74), 56(100), 44(69), 29(53), 15(17); *N, N'*-dicarbonyl piperazine: 142 M^+(38), 114(56), 85(52), 69(72), 56(100), 44(64), 29(32), 15(14).

[b] The individual products are detected by HNMR (δ, $CDCl_3$) analysis: *N*-methoxyl piperazine: **a**3.668(3H, s, -OCH_3), **b**3.372(4H, m, -CH_2), **c**2.689(4H, m, -CH_2), **d**1.897(1H, s, -NH); *N*-carbonyl piperazine: **a**8.027(H, s, -OCH), **b**3.511(2H, d, -CH_2), **c**3.364(2H, d, -CH_2), **d**2.872(2H, d, -CH_2), **e**2.822(2H, d, -CH_2), **f**2.003(1H, s, -NH); *N, N'*-dicarbonyl piperazine: **a** 8.474(2H, s, -OCH), **b**3.629(8H, s, -CH_2).The position of H atom in the products is shown in Fig. 5.

[c]Current efficiency is calculated by the following equations: $\eta = \frac{Q_t}{Q_p} \times 100\%$ (1); $Q_t = \frac{m}{M} ZF$ (2); $Q_p = \int_0^t Idt$ (3); where η is the current efficiency, Q_t is the theoretic electric quantity, Q_p is the practical electric quantity, m is the mass of product, M is the molar mass of product, Z is the charge number passed on the reaction, F is the faraday constant, I is the current passed on the reaction and t is

the reaction time.

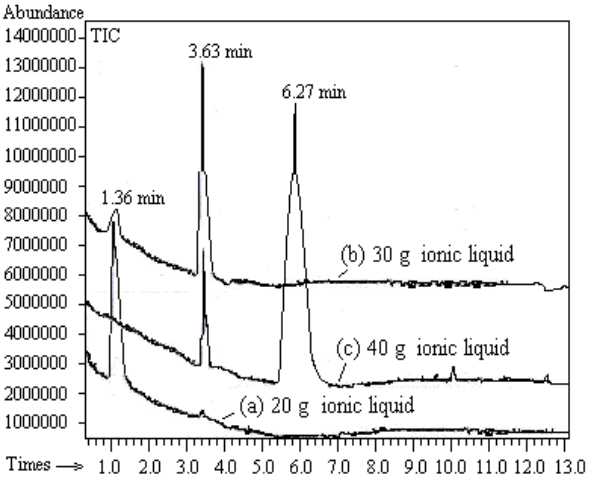

Figure 4. The representative graph of the GC results (the peak of the solvent has been omitted)

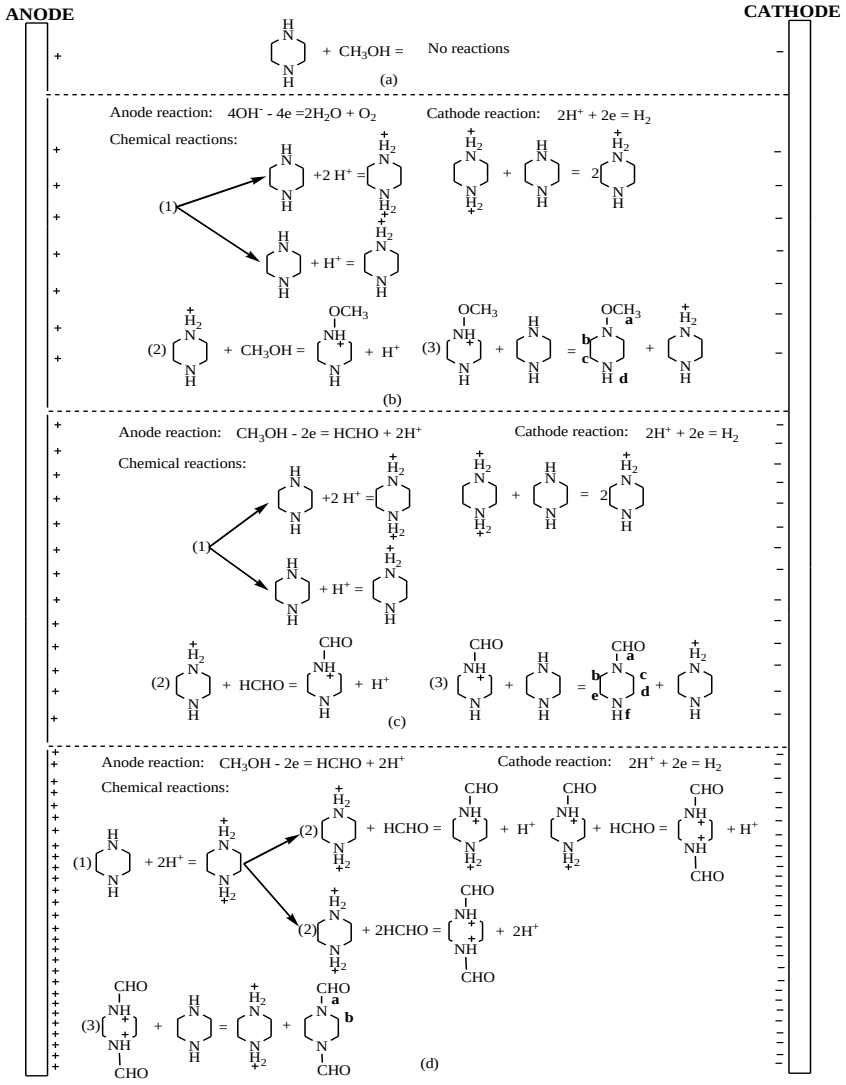

Figure 5. The possible reactions of the products: (a) without ionic liquid, (b) *N*-methoxyl piperazine, (c) *N*-carbonyl piperazine, (d) *N*, *N'*-dicarbonyl piperazine

3.3 Weight loss studies

Prior to the weight loss and polarization studies, the products are purified twice by vacuum distillation and are detected by HNMR. In the weight loss study, the HP13Cr steel specimen size is 5.0 × 2.0 × 0.4 cm, the testing temperature is 60 °C, the time is 4 h and the solution is 20% HCl. The inhibition efficiency (*IE*) is determined by equation (4), [22-29] where W_1 and W_2 are the weight loss values in the absence and presence, respectively, of a carbonyl piperazine inhibitor. The calculated results of equation (4) are shown in Table 2. According to Table 2, *N*-carbonyl piperazine and *N, N'*-dicarbonyl piperazine exhibit excellent inhibition efficiency, but piperazine and *N*-methoxyl piperazine have no inhibition effect on the corrosion of HP13Cr.

$$\mathrm{IE}(\%) = \frac{W_1 - W_2}{W_1} \times 100\% \quad (4)$$

Table 2. Weight loss and polarization results of HP13Cr steel corrosion in 20% HCl with and without adding 3% (weight %) inhibitors[d]

Inhibitor	Method						
	Weight loss		Polarization				
	W_{corr} (mg cm^{-2} h^{-1})	IE (%)	-E_{corr} VS. SCE(mV)	-b_c (mVdec^{-1})	b_a (mVdec^{-1})	I_{corr} (mA cm^{-2})	IE (%)
Blank	73.590	\	417	185	190	4.71	\
Piperazine	61.758	16.1	405	231	249	4.46	5.3
N-methoxyl piperazine	72.793	1.1	401	163	187	4.34	7.8
N-carbonyl piperazine	6.601	91.0	373	139	111	3.96	91.6
N,N'-dicarbonyl piperazine	4.642	95.2	356	125	99	0.059	98.8

[d] The weight loss testing temperature is 60 °C, the time is 4 h and the solution is 20% HCl.

3.4 Polarization

In the polarization study, epoxy resin is embedded in the HP13Cr steel specimen with φ 10 × 4 mm after being connected to copper wire on one side, and the exposure area in the electrolyte solution is 0.785 cm^2. Before all measurements were made, the samples were polished mechanically by abrasive papers from 300 mesh to 1200 mesh. Then, they were rinsed with acetone and double distilled water and were then soaked in the experimental solution. A solution of 20% HCl was prepared by the dilution method using 37% HCl solution as an analytical stage. A platinum electrode was used as the opposite electrode, and a saturated calomel electrode (SCE) was used as the reference electrode. The polarization was ±150 mv, and the scanning rate was 2 mV/s. All experiments were performed under unstirred atmospheric conditions, maintaining the temperature at 60 °C.

Fig. 6 shows the polarization curves of HP13Cr steel in 20% HCl solution. The corrosion

potential (E_{corr}), corrosion current density (I_{corr}), anode tafel slope (b_a), cathodic tafel slope (b_c) and corrosion inhibition efficiency (*IE*, %) are calculated by fitting the polarization curve. The results are shown in Table 2. According to the relation given by equation (5), [30-34] the inhibition efficiency is calculated. The corrosion current densities of I_{corr} and I'_{corr} are uninhibited and inhibited, respectively. They are determined by extrapolating the tafel line of the corresponding corrosion potential. As shown in Table 2, *N*-carbonyl piperazine and *N*, *N'*-dicarbonyl piperazine, which are calculated from the polarization curves, show excellent inhibition efficiency. However, piperazine and *N*-methoxyl piperazine show no effect on inhibiting the corrosion of HP13Cr. This is consistent with the weight loss results.

$$IE(\%) = (\frac{I_{corr} - I'_{corr}}{I_{corr}}) \times 100 \quad (5)$$

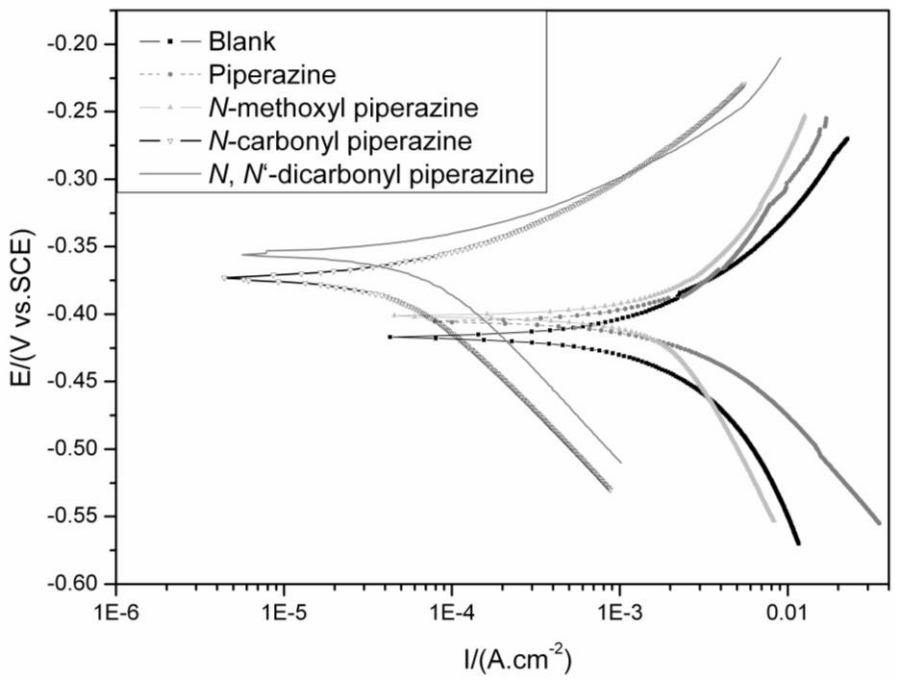

Figure 6. Polarization curves for HP13Cr steel in 20% HCl solution without and with different inhibitors.

Fig. 7 is a schematic diagram for the adsorption of the inhibitors on the metal surface. The better inhibition effects of *N*-carbonyl piperazine and *N*, *N'*-dicarbonyl piperazine is due to the lone electron pairs that are present on the O atom of the carbonyl group, which can enter the unoccupied d_{sp} hybridization orbits of the Fe atom to form the chelate compound, ultimately favoring the adsorption of the molecules on the metal surface. The adsorbed compounds block the interaction between the corrosion media and the metal substrate and therefore protect the metal surface from dissolution. Indeed, the N atom also has lone electron pairs, but they reside in the NH_2 groups of piperazine and *N*-methoxyl piperazine. The NH_2 group in HCl solution can rapidly form the quaternary ammonium compound by combining with the HCl, and the quaternary ammonium compound tends to adsorb onto

the metal surface via electrostatic interactions. However, adsorption is very sensitive to temperature. The adsorption weakens as temperature increases, and thermal desorption will occur easily at higher temperatures. Furthermore, the ionization potential value of methoxyl (approximately 10.8 eV) is higher than that of the aldehyde group (approximately 10.2 eV), resulting in the weaker adsorption of methoxyl compared to the aldehyde group. As a result of these factors, the inhibition effect of *N*-methoxyl piperazine is lower than those of *N*-carbonyl piperazine and *N, N'*-dicarbonyl piperazine.

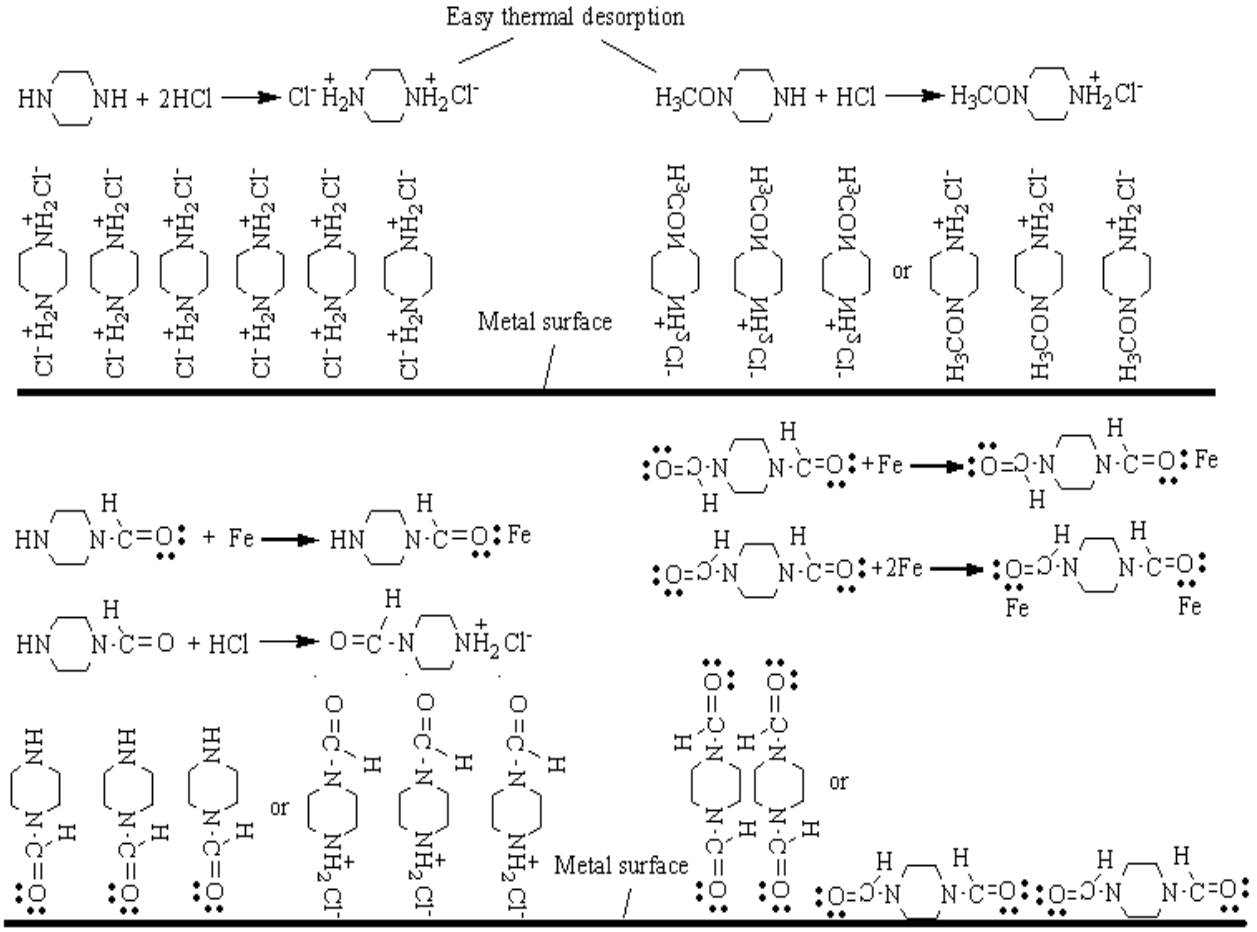

Figure 7. Schematic diagram for the adsorption of the inhibitors on the metal surface.

4. CONCLUSION

Three different products are synthesized by adjusting the quantity of ionic liquid [Bmim][PF_6] and current density in the electrochemical oxidation of piperazine. As determined by GC/MS and HNMR, the molecular structures of the three products are *N*-methoxyl piperazine, *N*-carbonyl piperazine, and *N, N'*-dicarbonyl piperazine. When the critical amount of ionic liquid [Bmim][PF_6] exceeds 30 g, the product is carbonyl piperazine. For application, the inhibition efficiencies of the three products on the corrosion of HP13Cr steel in 20% (weight %) HCl solution was studied by weight loss and polarization measurements. The experimental results reveal that *N*-carbonyl piperazine and *N, N'*-

dicarbonyl piperazine respectively exhibit 91.0% and 95.2% inhibition efficiencies at a concentration of 3% (weight %), whereas *N*-methoxyl piperazine shows no inhibition effect.

ACKNOWLEDGEMENTS

This work was supported by Social Development Science and Technology Project of Shaanxi Province (2016SF-429), the Youth Science and Technology Star of Shaanxi Innovation Talent Recommendation Program (2018KJXX-071) and Basic Research and Strategic Reserve Technology Research Fund Project of China National Petroleum Corporation (2018Z-01).

References

1. A.F. Zanette, I. Zampakidi, G.T. Sotiroudis, M. Zoumpanioti, I.C.R. Leal, R.O.M.A. de Souza, L. Cardozo-Filho, A. Xenakis, *J. Mol. Catal. B: Enzym.*, 107 (2014) 89.
2. Z.Yang, W.B. Pan, Enzyme Microb. *Tech.*, 37 (2005) 19.
3. I. Kaleem, H. Shen, B. Lv, B. Wei, A. Rasool, C. Li, *Chem. Eng.Sci.*, 106 (2014) 136.
4. Y.B. Wei, Q Zhao, Q.Q. Wu, H. Zhang, W.B Kong, J.Y. Liang, J. Yao, J. Zhang, J.L. Wang, *Carbohyd. Polym.*, 203 (2019) 157.
5. D. Zhao, M. Wu, Y. Kou, E. Min, *Catal. Today*, 74 (2002) 157.
6. X.D. Lang, Z.M. Li, L.N. He, *Catal. Today*, 324 (2019) 167.
7. B. Dong, W.J. Wang, W. Pan, G.J. Kang, *Mater. Chem. Phys.*, 226 (2019) 244.
8. Y.Q. Cui, L.L. Cheng, C.N. Wen, Y.T. Sang, P.Z. Guo, X.S. Zhao, *Colloids Surf. A*, 508 (2016) 173.
9. H. Kokubo, R. Sano, K. Murai, S. Ishii, M. Watanabe, *Eur. Polym. J.*, 106 (2018) 266.
10. O. Lebedeva, D. Kultin, N. Root, F. Guseynov, S. Dunaev, F.D. Melo, L. Kustov, *Synthetic Met.*, 221 (2016) 268.
11. M. Hirao, H. Sugimoto, H. Ohno, *J. ElectroChem. Soc.*, 147 (2000) 4168.
12. N. Muhammad, Y.A. Elsheik, M.I.A. Mutalib, A.A. Bazmi, R.A. Khan, H. Khan, S. Rafiq, Z. Man and I. Khan, *J Ind. Eng. Chem.*, 21 (2015) 1.
13. W.G. Birolli, I.M. Ferreira, N. Alvarenga, D. de A. Santos, I.L. de Matos, J.V. Comasseto, A.L.M. Porto, Biotechnol. Adv., 33 (2015) 481.
14. P. Lozano, J.M. Bernal, C. Gómez, E. García-Verdugo, M.I. Burguete, G. Sánchez, M. Vaultier, S.V. Luis, *Catal. Today*, 255 (2015) 54.
15. B.L. Gadilohar, G.S. Shankarling, *J. Mol. Liq.*, 227 (2017) 234.
16. Y.H. Yu, A.N. Soriano, M.H. Li, *J. Taiwan Inst. Chem. Eng.*, 40 (2009) 205.
17. R.L. Perry, K.M. Jones, W.D. Scott, Q. Liao, C.L. Hussey, *J. Chem. Eng. Data*, 40 (1995) 615.
18. J. Zhou, M.C. Ye, Z.Z. Huang, Y. Tang, *J. Org. Chem.*, 69 (2004) 1309.
19. R. Pacheco, A. Karmali, M.L. M. Serralheiro, P.I. Haris, *Anal. Biochem.*, 346 (2005) 49.
20. M.W. Martina, D.R. Lancia Jr., H.B. Li, S.E.R. Schiller, A.V. Toms, Z.G. Wang, K.W. Baira, J. Castro, S. Fessler, D. Gotur, S.E. Hubbs, G.S. Kauffman, M. Kershaw, G.P. Luke, C. McKinnon, L.L. Yao, W. Lu, D.S. Millan, *Bioorg. Med. Chem. Lett.*, 29 (2019) 1001.
21. T. Chonan, H. Tanaka, D. Yamamoto, M Yashiro, T. Oi, D. Wakasugi, A.O. Sugita, F. Io, H. Koretsune, A. Hiratate, *Bioorg. Med. Chem. Lett.*, 20 (2010) 3965.
22. M.P. Desimone, G. Grundmeier, G. Gordillo, S.N. Simison，*Electrochim. Acta*，56 (2011) 2990.
23. D. Thirumalaikumarasamy, K. Shanmugam, V. Balasubramanian, *J. Magnesium Alloys*, 2 (2014) 36.
24. R.T. Loto, *S. Afr. J. Chem. Eng.*, 24 (2017) 148.
25. J. Li, C.W. Du, Z.Y. Liu, X.G. Li, M. Liu, *Constr. Build. Mater.*, 189 (2018) 1286.
26. T.L. Zhao, Z.Y. Liu, C.W. Dua, M.H. Sun, X.G. Li, *Int. J. Fatigue*, 110 (2018) 105.
27. Y.C. Liu, B. Zhang, Y.L. Zhang, L.L. Ma, P. Yang, *Eng. Failure Anal.*, 60 (2016) 307.

28. T. Maertena, R. Oltra, C. Jaoul, C. Le Niniven, P. Tristant, F. Meunier, O. Jarry, *Surf. Coat. Technol.*, 363 (2019) 344.
29. V. Shkirskiy, P. Keil, H. Hintze-Bruening, F. Leroux, P. Volovitcha, K. Ogle, *Electrochim. Acta*，184 (2015) 203.
30. I Marco, O.V. der Biest, *Corros. Sci.*, 102 (2016) 384.
31. L.A. Shaik, S.K. Thamida, *Materialia*, 2 (2018) 183.
32. T. Bellezze, G. Giuliani, G. Roventi, *Corros. Sci.*, 130 (2018) 113.
33. W.J. Kuang, J.A. Mathews, D.D. Macdonald, *Electrochim. Acta*，127 (2014) 79.
34. Y. Xu, J.M. Sykes, *Prog. Org. Coat.*, 74 (2012) 549.